Supplementary Information

Electron Cloud Migration Effect Induced Lithiophobicity/Lithiophilicity Transformation for Dendrite-Free Lithium Metal Anodes

Wenyuan Zou,‡[a] Qianyao Li,‡[a] Zhe Zhu,[a] Lulu Du,[a] Xinyin Cai,[a] Yiming Chen,[a] Gang Zhang,[a] Song Hu,[a] Feilong Gong,[c] Lin Xu,*[a, b] and Liqiang Mai[a, b]

[a]State Key Laboratory of Advanced Technology for Materials Synthesis and Processing, School of Materials Science and Engineering, Wuhan University of Technology, Luoshi Road 122, Wuhan, 430070, P. R. China.
[b]Foshan Xianhu Laboratory of the Advanced Energy Science and Technology Guangdong Laboratory, Foshan 528200, China.
[c]Key Laboratory of Surface and Interface Science and Technology, Zhengzhou University of Light Industry, Zhengzhou, 450002, Henan, P. R. China.
*Corresponding Authors
E-mail: linxu@whut.edu.cn

Electrochemical Measurements: To test the cycling performance, the symmetrical cells (CR2016 coin cells) were produced in a glove box (argon atmosphere). Li@Cu-Ni, Li@NF and Li@CF composite anodes were used as electrodes in the symmetrical cells. The electrolyte (60 μL) consists of 1 mol L^{-1} bis(trifluoromethane)sulfonimide lithium salt (LiTFSI) in 1,2-dimethoxyethane (DME)/1,3-dioxolane (DOL, volume ratio: 1:1) and 2 wt% $LiNO_3$. For the coulombic efficiency test, a fixed capacity of Li (1 mAh cm^{-2}) was deposited by discharge at a constant current density and then charged to 1 V (LAND electrochemical testing system). The cyclic voltammetry was characterized by multi-channel electrochemical workstation (Bio-Logic SAS VMP-3). In order to test the full cell performance, $LiFPO_4$ (LFP) was chosen as the cathode material. LFP, Super P and polyvinylidene fluoride (PVDF) were added to N-methyl-2-pyrrolidone (NMP) in a ratio of 8:1:1. The mixture solution was scraped evenly onto the aluminium foil. Then the mixture was dried in a vacuum oven at 70 °C for 36 hours. Li@Cu-Ni, Li@NF and Li@CF composite anodes (3 mAh cm^{-2} Li) were reassembled to prepare full cells with LFP cathode. $LiPF_6$ (1 mol L^{-1}) in ethylene carbonate (EC) and dimethyl carbonate (DMC, volume ratio: 1:1) was selected as electrolyte (60 μL). The full cells were first cycled at 2.4-4 V at 0.1 C for three cycles for cell aging and activation. The cyclic stability of full cells was measured by setting a charging and discharging voltage range of 2.4-4 V and a current density of 0.5 C. Electrochemical impedance spectroscopy (EIS) was tested by assembling symmetrical cells from 0.1 Hz to 1 MHz with an amplitude of 10 mV via Autolab PGSTAT302N. The activation energy (E_a) was calculated by fitting EIS of symmetrical cells at different temperatures (10-60 °C) based on the Arrhenius formula:

$$\frac{1}{R}=A\exp\left(-\frac{E_a}{kT}\right) \qquad (1)$$

where R was the charge-transfer resistance at different temperatures from 10~60 °C, A was pre-exponential factor, E_a was activation energy, k was Boltzmann constant, and T was the temperature of testing process.

Computational Methods: All the calculation results were achieved by using density functional theory (DFT) with ultrasoft pseudopotential, plane-wave basis and periodic boundary conditions adopted in CASTEP. The optimized geometry structures were acquired with a force and energy convergence criterion less than 0.03 eV/Å and 10^{-6} au, respectively. The GGA-PBE and a 420 eV cut-off energy were employed for geometric optimization and property calculation. A 3×3×1 *k*-point was set to sample the Brillouin zone. Cu/Ni/Cu-Ni with (001) facet was modeled by a 3x3 super cell slab with 18 atoms. A 15 Å vacuum space was implemented to remove the periodicity in the z direction, while it was infinite in xy plane. The simulated systems under investigation consisted of a 10.844×10.844×18.615 Å Cu super cell, 10.572×10.572×18.524 Å Ni super cell, 10.572×10.572×18.524 Å Cu-Ni super cell, respectively. It was found that there was no fluctuation for total energy with the vacuum increasing. The adsorption energies (E_{ad}) of Li onto the crystals were calculated based on the description in literature;

$$E_{ad} = E(_{crystal+Li}) - E(_{crystal}) - E_{Li} \qquad (2)$$

where $E_{(crystal+Li)}$ and $E_{(crystal)}$ were the final energies of intrinsic Cu/Ni/Cu-Ni with and without Li atom; E_{Li} is the energy of a Li atom in the supercell.

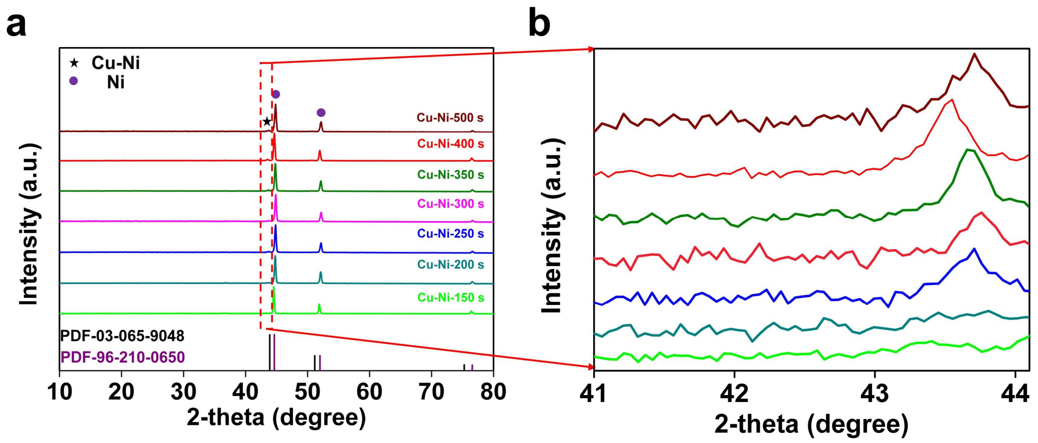

Fig. S1 a) XRD pattern of Cu-Ni with different electroplating time at 0.75 V. b) detailed XRD pattern of Cu-Ni with different electroplating time at 0.75 V.

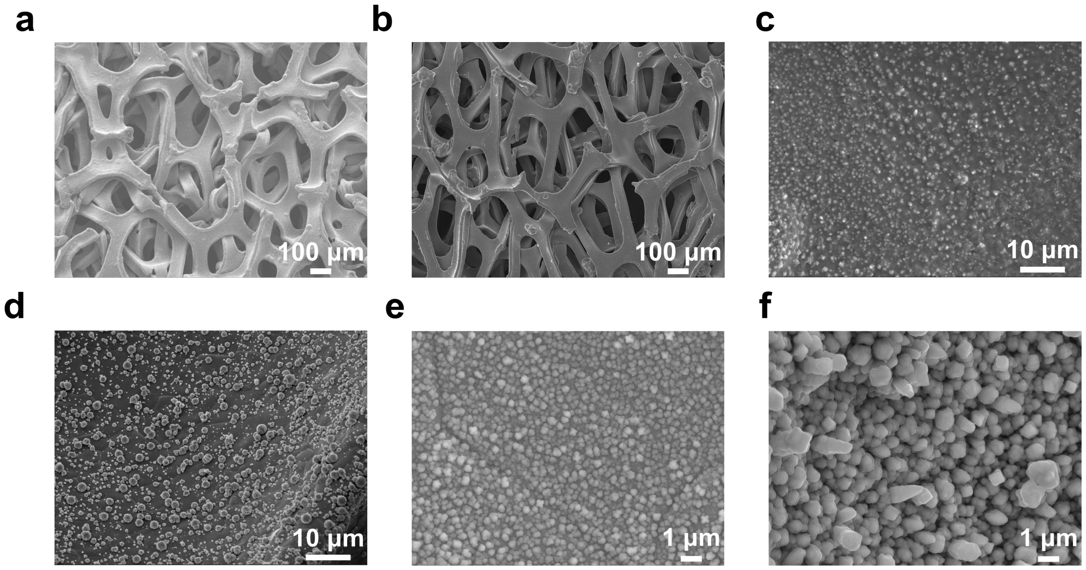

Fig. S2 SEM images of a) CF and b) NF. SEM images of different plating times: c) 250 s, d) 300 s, e) 400 s, f) 500 s.

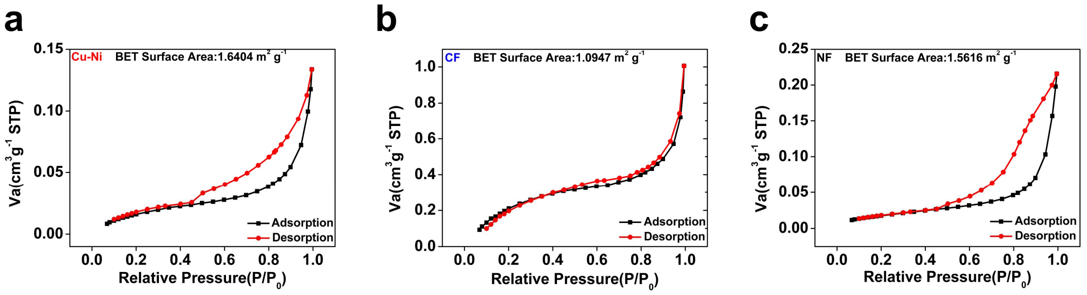

Fig. S3 Nitrogen adsorption-desorption isotherms of a) Cu-Ni, b) CF and c) NF. In order to reduce the error, Cu-Ni, CF and NF were all cut into 1 cm diameter disks for testing, and the number of disks used for testing is consistent.

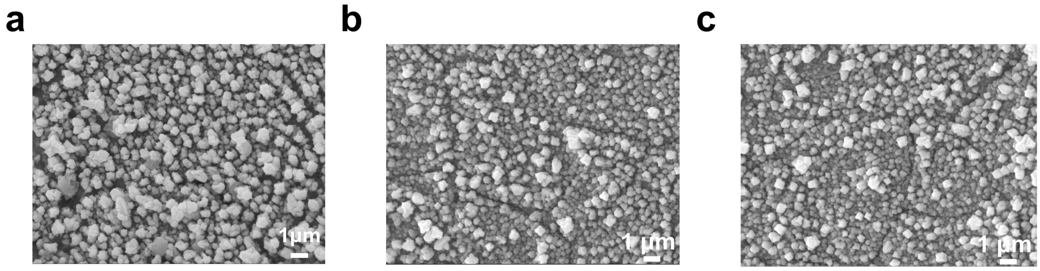

Fig. S4 SEM images of Cu-Ni synthesized under different electroplating voltages: a) 0.75 V, b) 0.7 V and c) 0.8 V.

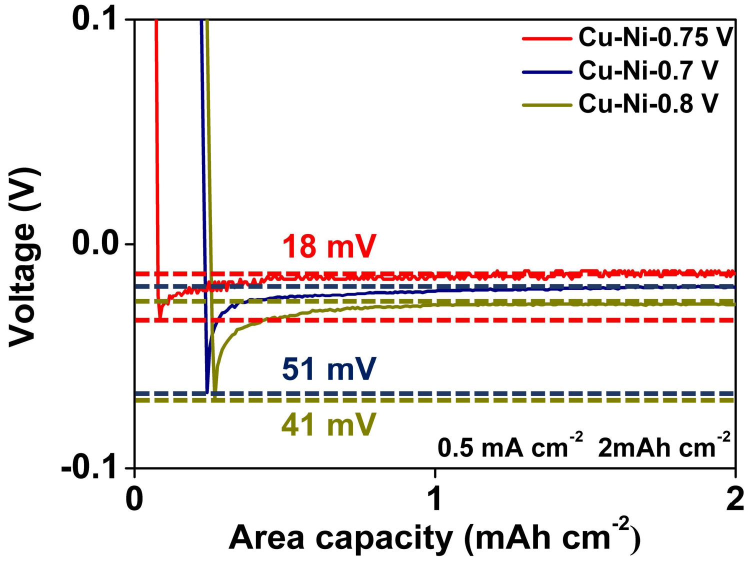

Fig. S5 Nucleation overpotential of galvanostatic Li deposition on Cu-Ni substrate at different electroplating voltage (0.7 V, 0.75 V, 0.8 V).

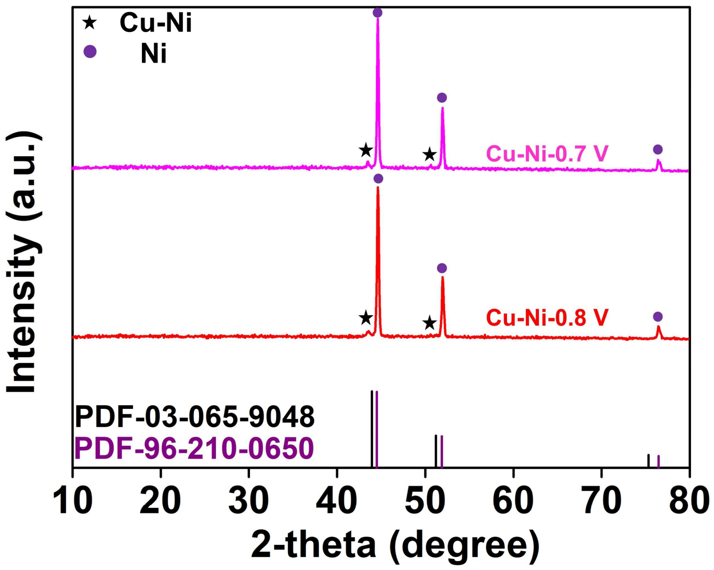

Fig. S6 XRD of Cu-Ni with different electroplating voltages (0.7 V and 0.8 V).

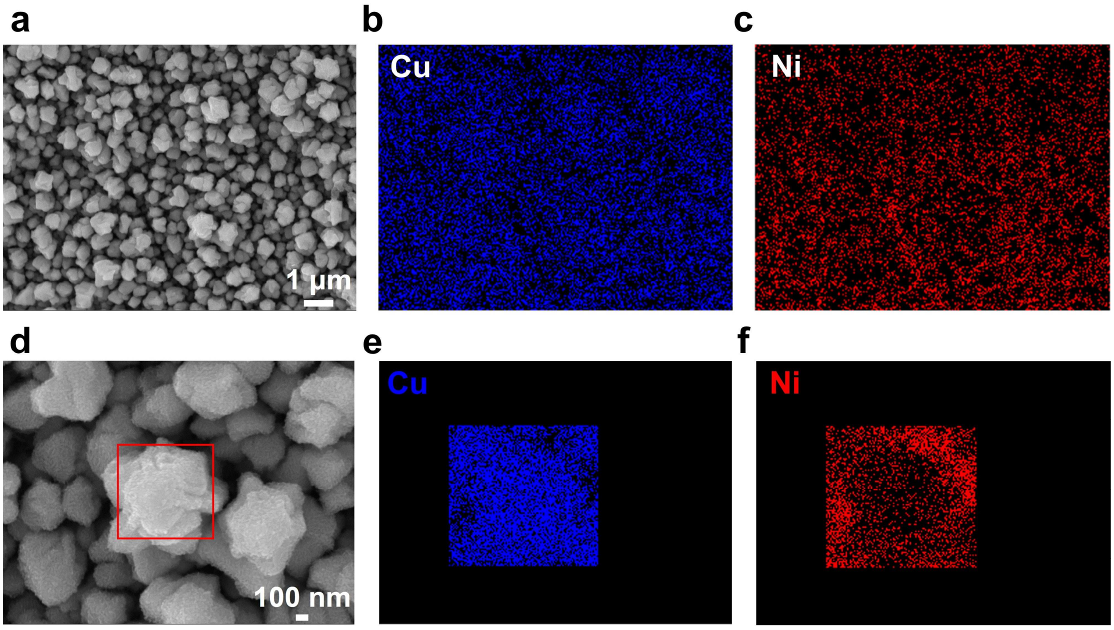

Fig. S7 a) SEM images of Cu-Ni. b, c) EDS mapping results of Cu-Ni. d) Magnification image of Cu-Ni and e, f) corresponding EDS mapping results.

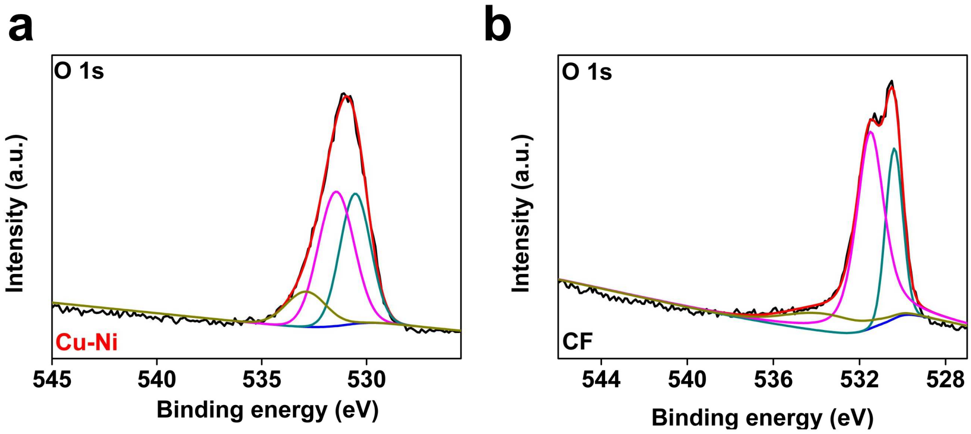

Fig. S8 O 1s XPS spectra of a) Cu-Ni, and b) CF. The O 1s spectrum of Cu-Ni is used to distinguish between Cu^0 and Cu_2O, which can be fitted into three peaks (530.54eV, 531.45eV, 532.88eV), corresponding to Cu_2O and a hydroxyl group or carbonate group and molecular water adsorbed on the surface, respectively. From the O 1s spectrum of Cu-Ni, we can deduce that there exists Cu_2O.[1]

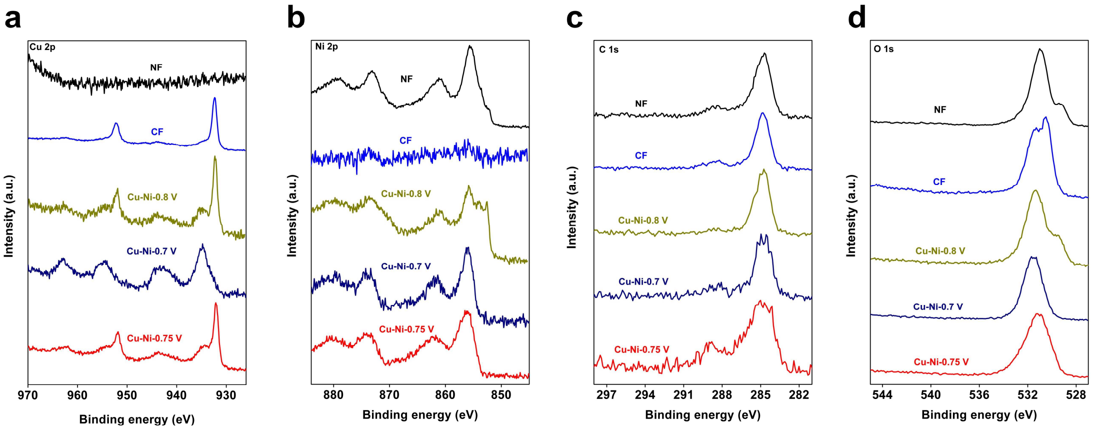

Fig. S9 XPS spectra of a) Cu 2p, b) Ni 2p, c) C 1s and d) O 1s in Cu-Ni-0.75 V, Cu-Ni-0.7 V, Cu-Ni-0.8 V, CF and NF.

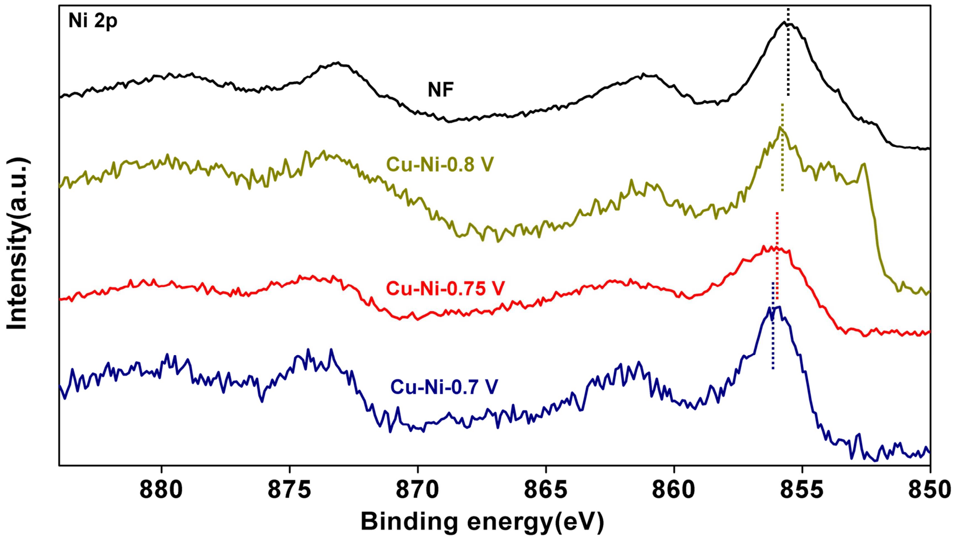

Fig. S10 Comparison of Ni 2p spectra in Cu-Ni-0.75 V, Cu-Ni-0.7 V, Cu-Ni-0.8 V and NF.

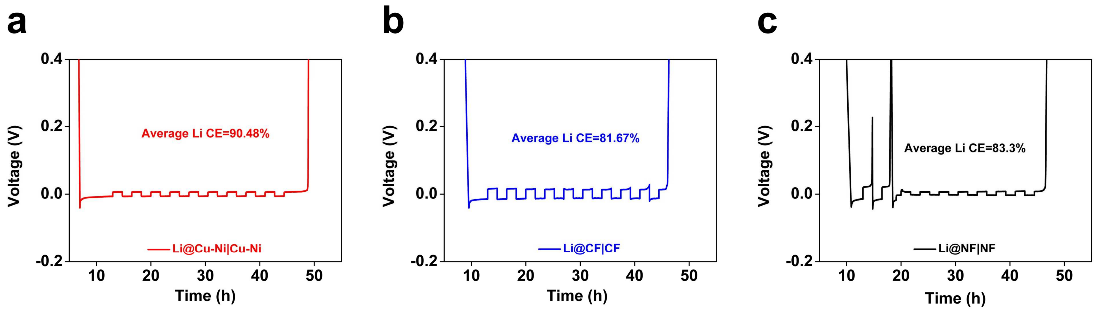

Fig S11 Voltage profiles of Li deposition/dissolution on a) Li@Cu-Ni|Cu-Ni, b) Li@CF|CF, and c) Li@NF|NF electrodes using the modified Aurbach method to determine the average Li CE.[2, 3] Briefly, a Li layer of 1.4 mAh cm^{-2} was deposited at 0.2 mA cm^{-2} on Cu-Ni, CF and NF, followed by ten cycles of Li deposition/dissolution of 0.35 mAh cm^{-2} and finally, stripping all the residual Li from the working electrode. The cut-off potential of Li stripping from the electrode was fixed at 1 V versus Li/Li^{+}. The average CE was calculated as follows:

$$The\ average\ CE = \frac{nQ_c+Q_s}{nQ_c + Q_p}$$

where n, Q_c, and Q_p represent cycle number, repeated Li striping/plating amount (0.35 mAh cm^{-2}), and initial Li plating amount (1.4 mAh cm^{-2}). Q_s is the final stripped amount of the residual Li after ten cycles of Li deposition/dissolution.

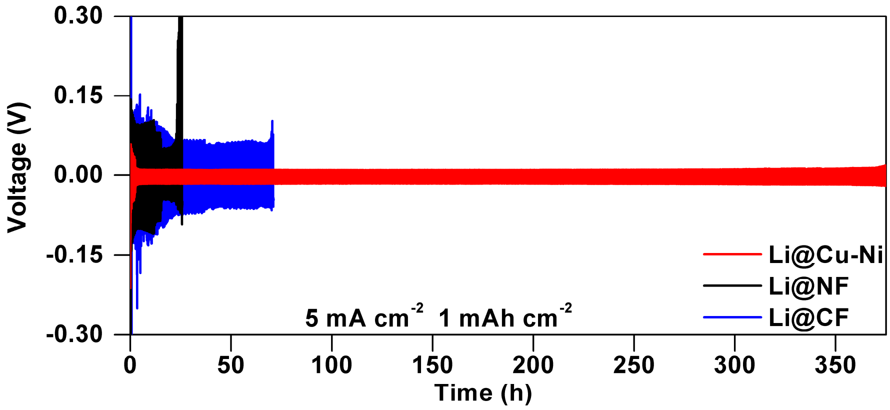

Fig. S12 Galvanostatic charge-discharge curves of Li@Cu-Ni|Li@Cu-Ni, Li@NF|Li@NF and Li@CF|Li@CF symmetrical cells at current density of 5 mA cm^{-2} with a cycling capacity of 1 mAh cm^{-2}.

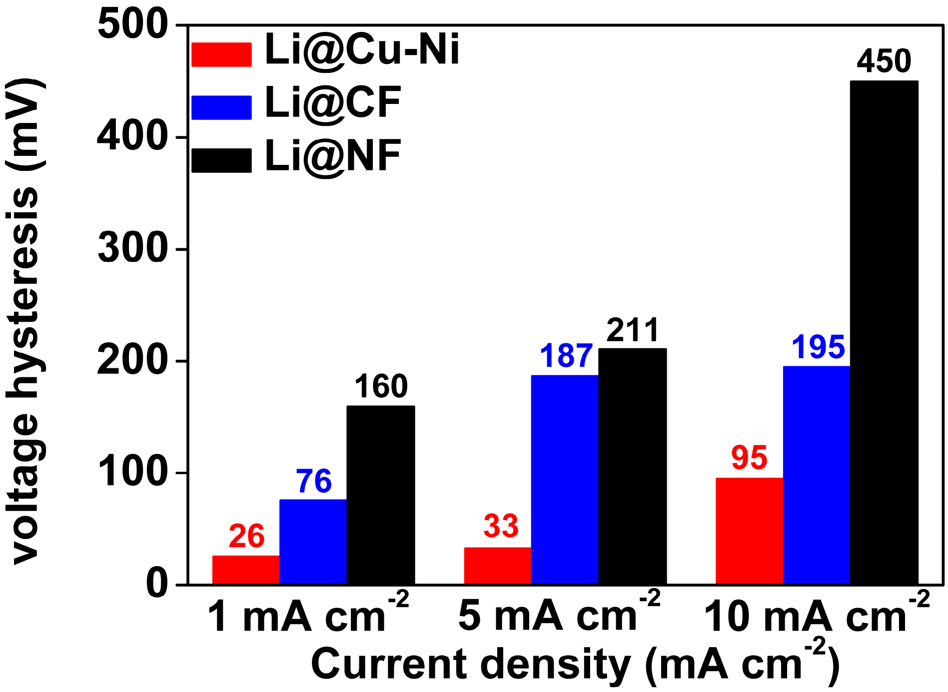

Fig. S13 The voltage hysteresis of Li@Cu-Ni, Li@CF and Li@NF under different current densities.

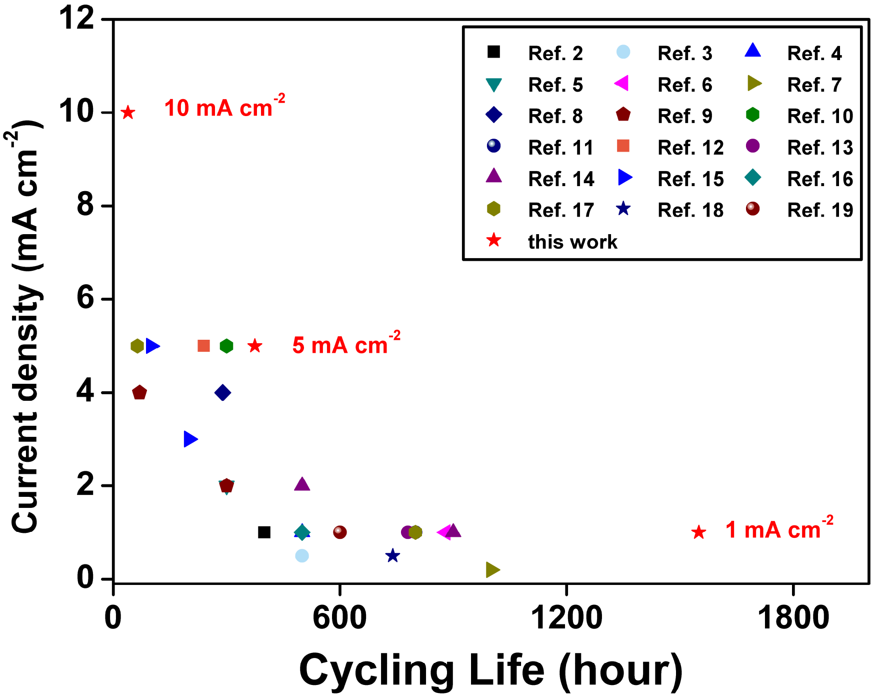

Fig. S14 Comparison of the cycling life of symmetrical cells using Li@Cu-Ni composite anodes and various reported Li metal-based composite anodes under various current density.

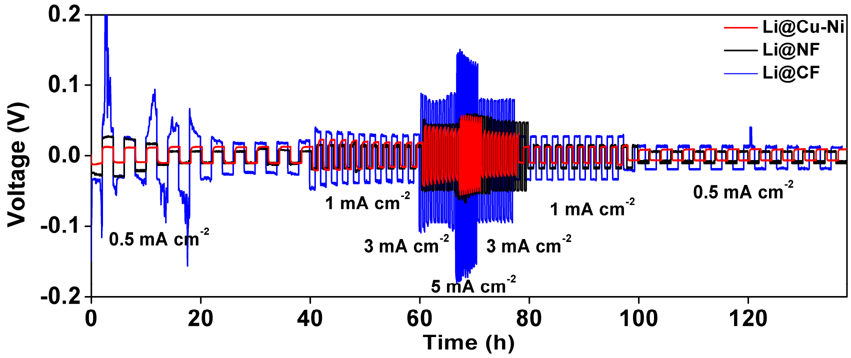

Fig. S15 Rate performances of Li@Cu-Ni, Li@NF and Li@CF symmetrical cells.

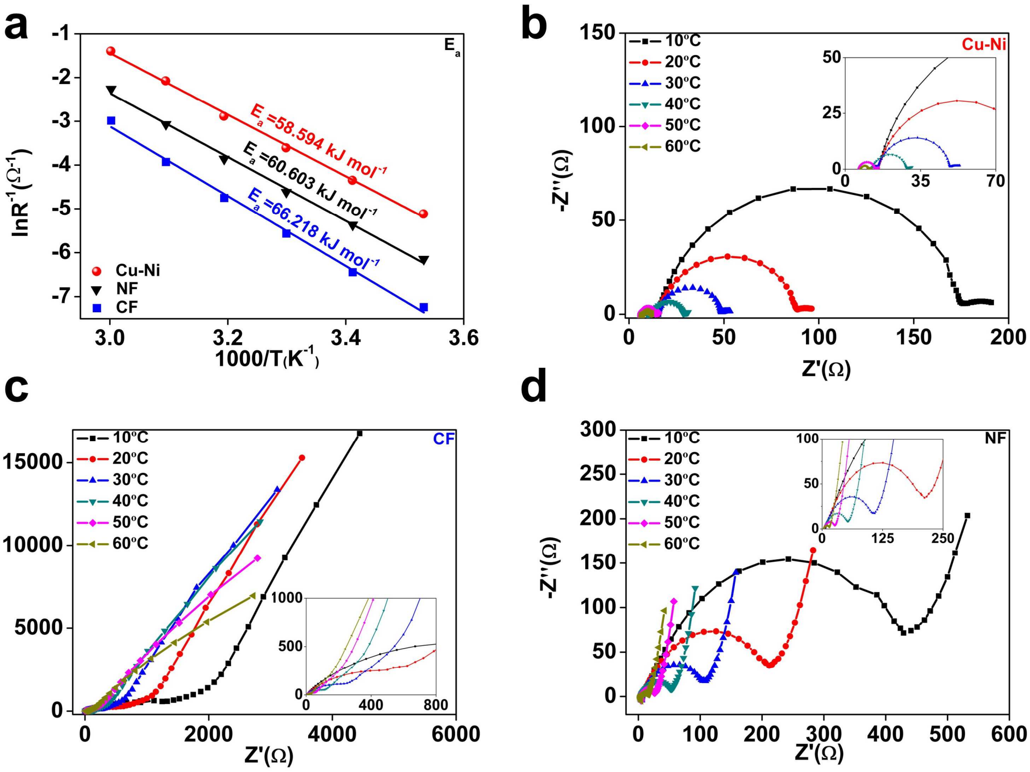

Fig. S16 a) Arrhenius curves and comparison of activation energies of Li@Cu-Ni, Li@CF and Li@NF. b) Nyquist plots of the Li@Cu-Ni|Li@Cu-Ni symmetrical cells at different temperatures. c) Nyquist plots of the Li@CF|Li@CF symmetrical cells at different temperatures. d) Nyquist plots of the Li@NF|Li@NF symmetrical cells at different temperatures. The activation energy (E_a) is calculated by fitting electrochemical impedance spectroscopy (EIS) of symmetrical cells at different temperatures (10-60 °C) based on the Arrhenius formula.

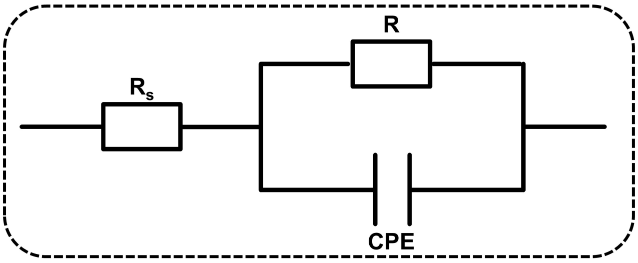

Fig. S17 The equivalent circuit models of the symmetrical cells at different temperatures.

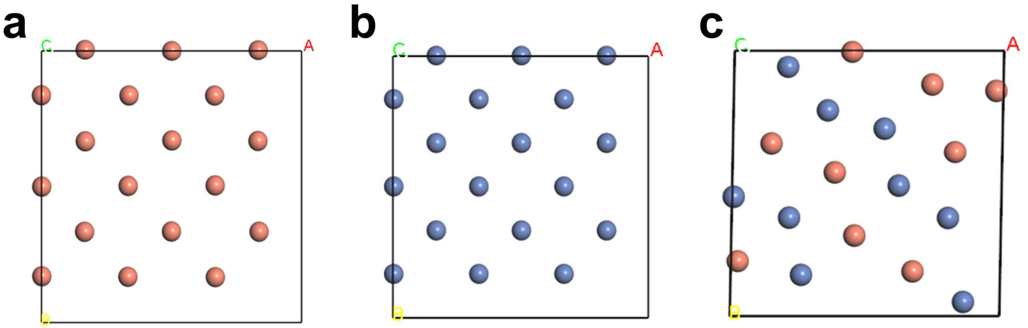

Fig. S18 The crystal models for a) Cu, b) Ni, and c) Cu-Ni.

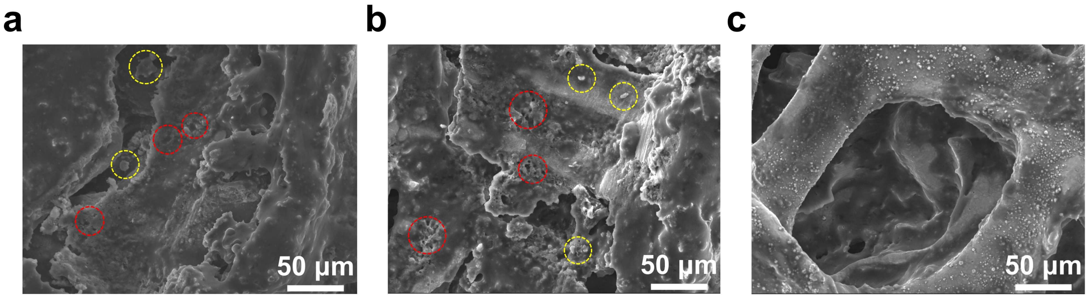

Fig. S19 Surface morphologies for Li@Cu-Ni, Li@CF and Li@NF composite anodes after 20 cycles: a) Li@CF; b) Li@NF; c) Li@Cu-Ni.

Table S1 The composition of Cu-Ni (0.75 V, 0.7 V, 0.8 V), CF and NF obtained by the XPS measurements.

	Cu:Ni	C (Atomic%)	O (Atomic%)	Cu (Atomic%)	Ni (Atomic%)
CF	**/**	**33.57**	**33.59**	**32.84**	**/**
NF	**/**	**22.76**	**45.38**	**/**	**31.86**
Cu-Ni-0.75 V	**1:1**	**21.85**	**47.75**	**14.52**	**15.87**
Cu-Ni-0.7 V	**1.5:1**	**25.48**	**47.58**	**16.51**	**10.43**
Cu-Ni-0.8 V	**0.5:1**	**37.08**	**36.37**	**8.24**	**18.31**

Table S2 Comparison of the cycle life of symmetrical cells using Li@Cu-Ni composite anodes and various reported Li metal-based composite anodes under various current density.

3D host for composite anode	Current density (mA cm^{-2})	Cycling capacity (mAh cm^{-2})	Cycling numbers	Cycling Life (hour)	Reference
Coralloid silver-coated carbon fiber network	1	1	200	400	[4]
AgNPs/carbon nanofiber	0.5	1	125	500	[5]
carbon cloth/CNT	1	1	250	500	[6]
MnO_2/graphene foam	2	1	300	300	[7]
3D duplex Cu	1	1	440	880	[8]
copper current collector with a 3D pore structure	0.2	1	100	1000	[9]
3D hybrid Cu framework with a lithophilic coating	4	1	580	290	[10]
Graphitized carbon fiber network	2	1	300	300	[11]
	4	1	140	70	
3D printed Cellulose nanofibers	5	2.5	300	300	[12]
single-atom Zn sites	1	1	400	800	[13]
Nitrogen, phosphorus codoped carbon cloth	5	1	600	240	[14]
gradient conductive-dielectric framework	1	1	390	780	[15]
g-C_3N_4@Ni foam	1	1	450	900	[16]
	2	1	500	500	

Co_3O_4-embedded and nitrogen-doped porous carbon nanoflake arrays on carbon fiber cloth	3	1	300	200	[17]
	5	1	250	100	
graphite-based layer modified nitrogen and sulfur co-doping carbon paper	1	1	250	500	[18]
Ni_xN decorated nickel foam	1	1	400	800	[19]
	5	1	160	64	
$AuLi_3$@Ni foam	0.5	1	185	740	[20]
3D porous Cu current collector	1	1	300	600	[21]
Li@Cu-Ni composite anode	1	1	529	1056	This work
	5	1	940	375	This work
	10	1	198	39	This work

Supporting Information Reference

1. J. J. Teo, Y. Chang and H. C. Zeng, *Langmuir*, 2006, **22**, 7369-7377.
2. B. D. Adams, J. M. Zheng, X. D. Ren, W. Xu and J. G. Zhang, *Adv. Energy Mater.*, 2018, **8**, 1702097.
3. Z. Peng, J. H. Song, L. Y. Huai, H. P. Jia, B. W. Xiao, L. F. Zou, G. M. Zhu, A. Martinez, S. Roy, V. Murugesan, H. Lee, X. D. Ren, Q. Y. Li, B. Liu, X. L. Li, D. Y. Wang, W. Xu and J. G. Zhang, *Adv. Energy Mater.*, 2019, **9**, 1901764.
4. R. Zhang, X. Chen, X. Shen, X. Q. Zhang, X. R. Chen, X. B. Cheng, C. Yan, C. Z. Zhao and Q. Zhang, *Joule*, 2018, **2**, 764-777.
5. C. P. Yang, Y. G. Yao, S. M. He, H. Xie, E. Hitz and L. B. Hu, *Adv. Mater.*, 2017, **29**, 1702714.
6. F. F. Liu, R. Xu, Z. X. Hu, S. F. Ye, S. F. Zeng, Y. Yao, S. Q. Li and Y. Yu, *Small*, 2019, **15**, 1803734.
7. B. Z. Yu, T. Tao, S. Mateti, S. G. Lu and Y. Chen, *Adv. Funct. Mater.*, 2018, **28**, 1803023.
8. K. Lin, T. Li, S. W. Chiang, M. Liu, X. Y. Qin, X. F. Xu, L. H. Zhang, F. Y. Kang, G. H. Chen and B. H. Li, *Small*, 2020, DOI: 10.1002/smll.202001784.
9. Q. B. Yun, Y. B. He, W. Lv, Y. Zhao, B. H. Li, F. Y. Kang and Q. H. Yang, *Adv. Mater.*, 2016, **28**, 6932-6939.
10. Y. M. Liu, X. Y. Qin, S. Q. Zhang, L. H. Zhang, F. Y. Kang, G. H. Chen, X. F. Duan and B. H. Li, *J. Mater. Chem. A*, 2019, **7**, 13225-13233.
11. T. T. Zuo, X. W. Wu, C. P. Yang, Y. X. Yin, H. Ye, N. W. Li and Y. G. Guo, *Adv. Mater.*, 2017, **29**, 1700389.
12. D. X. Cao, Y. J. Xing, K. Tantratian, X. Wang, Y. Ma, A. Mukhopadhyay, Z. Cheng, Q. Zhang, Y. C. Jiao, L. Chen and H. L. Zhu, *Adv. Mater.*, 2019, **31**, 1807313.
13. K. L. Xu, M. G. Zhu, X. Wu, J. W. Liang, Y. Liu, T. W. Zhang, Y. C. Zhu and Y. T. Qian, *Energy Storage Mater.*, 2019, **23**, 587-593.
14. K. Li, Z. Y. Hu, J. Z. Ma, S. Chen, D. X. Mu and J. T. Zhang, *Adv. Mater.*, 2019, **31**, 1902399.
15. J. Li, P. C. Zou, S. W. Chiang, W. T. Yao, Y. Wang, P. Liu, C. W. Liang, F. Y. Kang and C. Yang, *Energy Storage Mater.*, 2020, **24**, 700-706.
16. Z. Y. Lu, Q. H. Liang, B. Wang, Y. Tao, Y. F. Zhao, W. Lv, D. H. Liu, C. Zhang, Z. Weng, J. C. Liang, H. Li and Q. H. Yang, *Adv. Energy Mater.*, 2019, **9**, 1803186.
17. G. Y. Jiang, N. Jiang, N. Zheng, X. Chen, J. Y. Mao, G. Y. Ding, Y. H. Li, F. G. Sun and Y. S. Li, *Energy Storage Mater.*, 2019, **23**, 181-189.

18. D. D. Li, S. S. Zhang, Q. Zhang, P. Kaghazchi, H. C. Qi, J. Liu, Z. Y. Guo, L. Wang and Y. G. Wang, *Energy Storage Mater.*, 2020, **26**, 593-603.
19. J. F. Zhu, J. Chen, Y. Luo, S. Q. Sun, L. G. Qin, H. Xu, P. G. Zhang, W. Zhang, W. B. Tian and Z. M. Sun, *Energy Storage Mater.*, 2019, **23**, 539-546.
20. X. Ke, Y. H. Liang, L. H. Ou, H. D. Liu, Y. M. Chen, W. L. Wu, Y. F. Cheng, Z. P. Guo, Y. Q. Lai, P. Liu and Z. C. Shi, *Energy Storage Mater.*, 2019, **23**, 547-555.
21. Q. Li, S. P. Zhu and Y. Y. Lu, *Adv. Funct. Mater.*, 2017, **27**, 1606422.